Publishing Excellence Inspiring Progress
ARISTON PUBLICATIONS
Quantum Advances
ISSN: 3143-0724 www.aristonpubs.com/journal/quantum-advances https://doi.org/10.69626/qa.2026.0036

RESEARCH ARTICLE

Effect of Gaussian, Bessel, and uniform laser fields on the electronic structure of single and double quantum rings under magnetic fields

Camilo Frías Viña[1], Fernando Guerrero Almanza[1], Juan Alejandro Vinasco[2*], J. Sierra-Ortega[1], Gene Elizabeth Escorcia-Salas[1]

ABSTRACT: We study the electronic properties of quantum ring systems under magnetic and intense nonresonant laser fields, considering both an ideal two-dimensional ring and a Kuroda-type double-ring structure. The laser field is modeled using constant, Gaussian, and Bessel profiles, which modify the effective confinement according to their spatial intensity distribution. In the single-ring case, the laser induces a transition from a ring-like regime, with oscillatory energy levels, to a quantum dot–like behavior with an almost linear dependence on the magnetic field. This transition depends on the laser profile. For the double-ring structure, the outer ring dominates the low-energy states, while the inner ring contributes at higher energies, leading to a combined spectral response. The laser mainly modifies the angular distribution of the electronic states without inducing transfer between rings, due to the breaking of azimuthal symmetry by the x-polarization.

Keywords: Quantum Rings; Magnetic Field; Non-resonant Laser Field; Gaussian Beam; Bessel Beam

Received: 21 December 2025; Revised: 19 February 2026; Accepted: 6 March 2026; Published Online: 15 March 2026

1. INTRODUCTION

Semiconductor quantum nanostructures have attracted considerable attention in recent years due to their tunable electronic and optical properties and their potential applications in optoelectronics, photonics, sensing, energy conversion, and quantum technologies [1–4]. Among these systems, quantum dots and quantum rings represent important low-dimensional platforms because quantum confinement strongly modifies the carrier dynamics, optical transitions, and transport properties at the nanoscale [5–7]. Recent developments in fabrication techniques have enabled the realization of nanostructures with increasingly complex geometries, including coupled quantum dots, toroidal systems, tetrapod structures, vertically stacked rings, and multiple concentric quantum rings [8–11]. These geometries introduce additional confinement regions and richer electronic behavior than conventional single quantum dots. The geometry of semiconductor nanostructures plays a fundamental role in determining their electronic and optical properties. Previous studies have shown that confinement anisotropy, finite barrier effects, and realistic structural profiles strongly influence energy spectra, wavefunction localization, optical absorption, and nonlinear optical responses [7, 12, 13]. In particular, coupled and multiring systems exhibit complex spectral structures due to the coexistence of different confinement regions and tunnel coupling effects [9, 14, 15]. Similar effects have also been reported in tetrapod and core/shell quantum dot systems, where geometry and confinement strongly

[1] Grupo de Investigación en Teoría de la Materia Condensada, Universidad del Magdalena, Santa Marta 470004, Colombia.

[2] Departamento de Ciencias Básicas, Facultad de Ingeniería y Administración, Universidad Nacional de Colombia, Palmira 763533, Colombia.

* Author to whom correspondence should be addressed: javinascos@unal.edu.co (J. A. Vinasco)

© Ariston Publications 2026. All rights reserved.

modify nonlinear optical rectification and harmonic generation processes [13, 16]. These properties make semiconductor nanostructures promising candidates for photonic devices, quantum information technologies, and optical switching applications [17]. The interaction between semiconductor nanostructures and external electric, magnetic, and optical fields has become an active area of research because these perturbations allow efficient control of carrier localization and confinement symmetry [6, 18, 19]. In quantum rings, magnetic fields induce oscillatory energy spectra associated with the Aharonov– Bohm effect and strongly modify the magnetic and optical response of the system [5, 20]. Electric fields, impurities, and spin-related interactions can additionally distort the spatial distribution of the confined carriers and modify the electronic localization [6, 18]. In particular, intense non-resonant laser fields provide an efficient mechanism for reshaping the effective confinement potential through laser dressing within the Kramers–Henneberger formalism [21–23].

Previous works have demonstrated that laser radiation can induce wavefunction redistribution, modify interband transitions, alter optical absorption, and generate transitions between ring-like and quantum dot–like confinement regimes [15, 19, 23]. Most theoretical studies involving laser-dressed quantum rings assume spatially uniform laser fields. However, realistic optical beams exhibit non-uniform intensity distributions capable of generating spatially dependent modifications of the confinement potential. In this context, structured optical fields such as Gaussian and Bessel beams have attracted increasing attention because they provide additional control over confinement symmetry and carrier localization [24]. On the other hand, experimentally fabricated quantum rings generally exhibit finite vertical extension and realistic toroidal profiles rather than idealized two-dimensional geometries [9, 25]. These realistic systems may contain multiple confinement regions associated with inner and outer rings, leading to additional spectral branches and more complex electronic localization. Consequently, understanding how structured laser fields modify realistic single and double quantum ring systems under magnetic confinement remains an open problem of both fundamental and technological interest. In this work, we investigate the electronic properties of single and double quantum ring systems under the combined influence of magnetic and intense non-resonant laser fields. Both an ideal two-dimensional quantum ring and a realistic Kuroda-type double-ring structure are considered [26]. The laser field is modeled using constant, Gaussian, and Bessel spatial profiles in order to analyze how the beam distribution modifies the effective confinement, the energy spectrum, and the spatial localization of the electronic states. In the theoretical framework section, the effective-mass approximation and the laser-dressed confinement model are introduced. Subsequently, the influence of the different laser profiles on the electronic states is analyzed as a function of the magnetic field.

2. THEORETICAL FRAMEWORK

The electronic properties of these systems were studied within the effective mass approximation in the presence of external magnetic and nonresonant intense laser fields. The time-dependent Schrödinger equation for a confined electron can be written as

$$\left[\frac{1}{2m^*}\Big(-i\hbar\nabla + e\mathbf{A}_m + e\mathbf{A}_L(t)\Big)^2 + V(\mathbf{r})\right]\Psi(\mathbf{r},t) = i\hbar\frac{\partial}{\partial t}\Psi(\mathbf{r},t) \tag{1}$$

where m^* is the electron effective mass, $V(\mathbf{r})$ represents the confinement potential, and $\mathbf{A}_m$ and $\mathbf{A}_L$ are the vector potentials associated with the magnetic and laser fields, respectively, and e elementary charge. The magnetic field was considered perpendicular to the ring plane, $\mathbf{B} = B\hat{z}$, and the symmetric gauge was adopted.

$$\mathbf{A}_m = \frac{B}{2}(-y, x, 0) \tag{2}$$

The nonresonant laser field was assumed to propagate perpendicular to the structure and to be linearly polarized along the x-direction.

$$\mathbf{A}_L(t) = A_0\cos(\omega t)\,\hat{x} \tag{3}$$

where A_0 and ω are the amplitude and angular frequency of the laser field, respectively. The laser effects were introduced through the Kramers-Henneberger transformation, which transforms the time-dependent problem into an effective time-independent equation,

© Ariston Publications 2026. All rights reserved.

$$\left[-\frac{\hbar^2}{2m^*}\nabla^2 + \frac{eB}{2m^*}i\hbar\left(x\frac{\partial}{\partial y} - y\frac{\partial}{\partial x}\right) + \frac{e^2B^2}{8m^*}(x^2+y^2) + V_d(\mathbf{r})\right]\Phi(\mathbf{r}) = E\Phi(\mathbf{r}) \tag{4}$$

where $V_d(\mathbf{r})$ is the laser-dressed confinement potential. The dressed potential is obtained from the time average of the original confinement profile along the laser polarization direction:

$$V_d(\mathbf{r}) = \frac{\omega}{2\pi}\int_0^{2\pi/\omega} V(x+\alpha(x,y)\cos(\omega t), y, z)\ dt \tag{5}$$

where $\alpha(x,y)$ is the laser parameter associated with the intensity of the incident radiation. In this work, constant, Gaussian, and Bessel laser profiles were considered in order to analyze how different spatial intensity distributions modify the effective confinement and the electronic states. The energy levels and wavefunctions were calculated numerically using the finite element method (FEM), which is suitable for systems with nonuniform confinement profiles and realistic geometries. Dirichlet boundary conditions were imposed at the external borders of the simulation region by taking the wavefunction equal to zero outside the confinement domain.

Figure 1 illustrates the geometries analyzed in this work. Panel (a) shows the ideal two-dimensional quantum ring, where the electron motion is confined to a planar annular region defined by inner and outer radii. This simplified model preserves full rotational symmetry and is commonly used as a reference system. In contrast, Figure 1 b presents a three-dimensional toroidal structure constructed from an experimentally reported profile. In this case, the ring exhibits a finite vertical extension and a smooth variation of its cross section, resulting in a more realistic confinement potential. Such geometries are typically obtained through droplet epitaxy techniques, where the final structure deviates from a strictly planar ring and forms a toroidal shape with measurable thickness. The comparison between both configurations allows us to evaluate the role of dimensionality and geometrical details on the electronic properties of the system. While the 2D model captures the essential physics associated with radial confinement, the 3D Kuroda - type

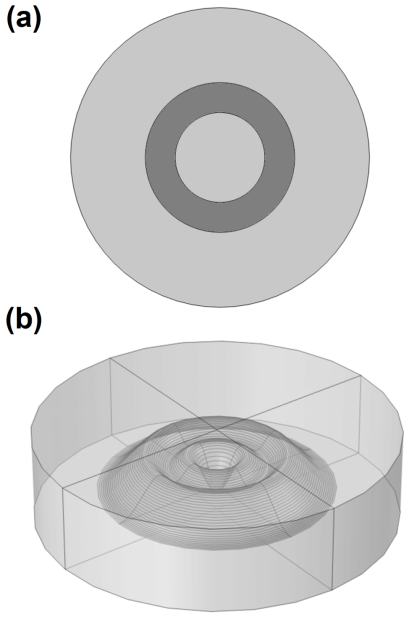

Fig. 1. Schematic representation of the systems considered in this work. (a) Ideal two-dimensional quantum ring defined by inner and outer radii, with confinement in a planar annular region. (b) Three-dimensional toroidal structure based on a Kuroda-type profile, characterized by a finite vertical extension and a non-uniform cross section.

structure incorporates additional features such as vertical confinement and curvature effects, which are expected to modify both the energy spectrum and the spatial distribution of the electronic states. In addition to the uniform laser field, spatially dependent laser profiles were considered in order to describe more realistic optical confinements. In this case, the laser parameter becomes position dependent and modifies the effective confinement according to the spatial distribution of the optical field. The Gaussian profile produces a smooth spatial confinement around the beam center, while the Bessel profile generates a radially varying confinement determined by the beam structure. Thus, the laser parameter was written as

$$\alpha(x,y) = \begin{cases} \alpha_0, & \text{for constant profile,} \\ \alpha_0 \exp\left[-\dfrac{(x-x_{\rm sh})^2+(y-y_{\rm sh})^2}{w^2}\right], & \text{for Gaussian beam,} \\ \alpha_0 J_0\left(\dfrac{2\pi}{\lambda}\sqrt{(x-x_{\rm sh})^2+(y-y_{\rm sh})^2}\right), & \text{for 0th-order Bessel beam.} \end{cases} \tag{6}$$

where $(x_{\rm sh}, y_{\rm sh})$ defines the beam center, w is the Gaussian width, λ is the characteristic spatial parameter associated with the Bessel beam, and J_0 denotes the zeroth-order Bessel function of the first kind.

© Ariston Publications 2026. All rights reserved.

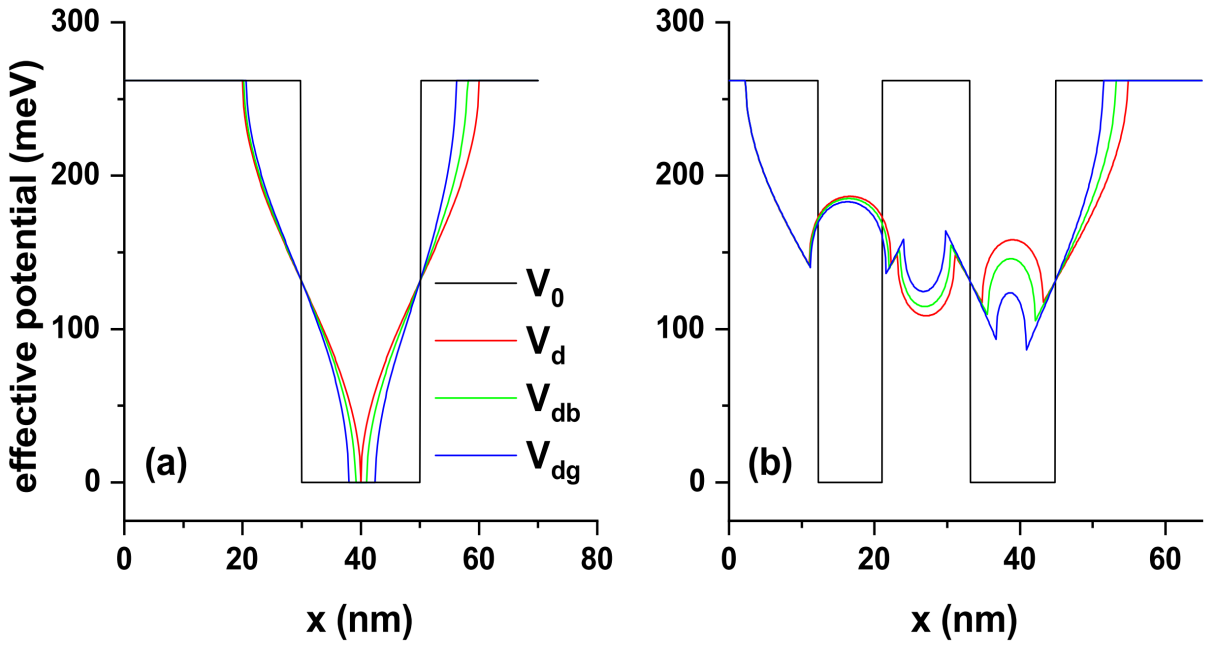

Fig. 2. Effective confinement potential along the xdirection for (a) the ideal 2D quantum ring and (b) the 3D Kuroda-type double-ring structure (evaluated at $z = 5$ nm). The black line (V_0) corresponds to the confinement potential without laser field. The red curve (V_d) represents a spatially uniform laser field, the green curve (V_{db}) corresponds to a Bessel beam, and the blue curve (V_{dg}) to a Gaussian beam. The laser parameter is fixed at $\alpha_0 = 10$ nm.

3. RESULTS AND DISCUSSION

For the numerical calculations, the effective masses were taken as $m^*_{\text{in}} = 0.063\, m_e$ for GaAs and $m^*_{\text{out}} = 0.093\, m_e$ for the AlGaAs barrier, where m_e is the free-electron mass. The confinement potential was defined by $V_{\text{in}} = 0$ inside the quantum ring and $V_{\text{out}} = 0.262$ eV outside the structure. For the ideal two-dimensional quantum ring, the inner and outer radii were fixed at $R_1 = 30$ nm and $R_2 = 50$ nm, respectively. The magnetic field was applied perpendicular to the ring plane along the z-direction. For the Gaussian beam, the width parameter was fixed at $w = 80$ nm, while for the Bessel beam the spatial parameter was chosen as $\lambda = 400$ nm. The laser beam center was located at $(x_{\text{sh}}, y_{\text{sh}}) = (0, 0)$. The numerical calculations were performed within a finite simulation region of radius $R_c = 100$ nm. All energy values reported throughout this work are given in meV.

Figure 2 shows the modification of the effective confinement potential induced by different laser profiles. Panel (a) corresponds to the ideal 2D quantum ring, while panel (b) presents the Kuroda-type double-ring structure, where the potential is evaluated at $z = 5$ nm in order to clearly resolve the presence of the inner and outer rings. In the absence of the laser field (black curve, V_0), the confinement exhibits a well-defined structure determined solely by the geometry of the system. In the 2D case, the potential forms a single annular well, whereas in the Kuroda structure two distinct confinement regions appear, corresponding to the inner and outer rings. When the laser field is introduced ($\alpha_0 = 10$ nm), the potential is modified depending on the spatial profile of the beam. For a spatially uniform field (red curve, V_d), the confinement is symmetrically renormalized, leading to a global smoothing of the potential without altering its overall shape. As a result, the electron experiences a slightly softened confinement, which can enhance its spatial delocalization. In contrast, structured laser profiles produce non-uniform modifications. The Gaussian beam (blue curve, V_{dg}) induces a stronger deformation near the central region of the system, effectively deepening the potential well and increasing localization of the electron around specific regions. The Bessel beam (green curve, V_{db}) introduces a spatially modulated potential, generating additional local minima and barriers along the radial direction. These effects are particularly evident in the Kuroda geometry (Figure 2 b), where the presence of two rings leads to a more complex response. The laser-induced modulation alters the relative depth of the inner and outer wells, which can favor electron localization in one ring over the other. This competition between confinement regions suggests that the spatial profile

 © Ariston Publications 2026. All rights reserved.

of the laser field provides an efficient mechanism to control the distribution of electronic states in multi-ring structures.

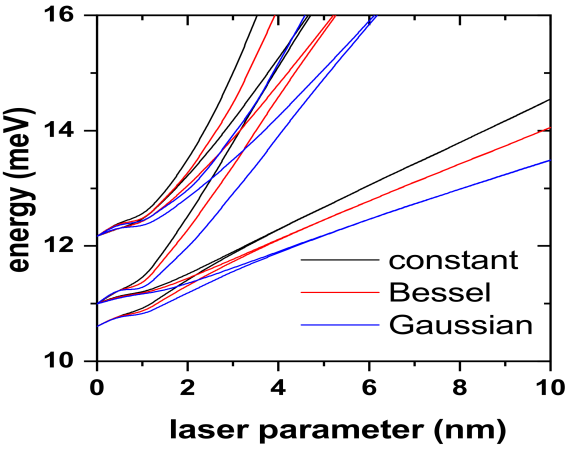

Fig. 3. Lowest electronic energy levels as a function of the laser parameter α_0 for different laser profiles. The black curves correspond to a spatially uniform (constant) laser field, while the red and blue curves represent Bessel and Gaussian beams, respectively. The quantum ring is defined by an inner radius of 30 nm and an outer radius of 50 nm, with the confinement region located between these two values.

Figure 3 shows the evolution of the lowest electronic energy levels as a function of the laser parameter α_0 for different laser profiles. The black curves correspond to a spatially uniform (constant) laser field, while the red and blue curves represent Bessel and Gaussian beams, respectively. As α_0 increases, all energy levels shift to higher values, indicating an effective strengthening of the confinement. This behavior arises from the modification of the effective potential induced by the laser field, which reduces the accessible region for the electron. For the constant laser field (black curves), the energy levels vary smoothly with α_0. This case provides a useful reference, although it assumes a uniform intensity distribution over the system. In contrast, Gaussian and Bessel beams introduce a spatial dependence in the laser intensity. The Gaussian profile, which is commonly used to describe laser beams in optical systems, concentrates most of the intensity near the center, leading to a stronger modification of the confinement in that region. As a result, the energy levels show a larger shift compared to the constant case. The Bessel beam presents a different spatial structure, with intensity distributed in a central peak surrounded by concentric rings. This radial modulation produces a non-uniform change in the confinement, leading to an intermediate behavior between the constant and Gaussian cases. These results show that, beyond the strength of the laser field, its spatial distribution plays an important role in determining the electronic structure. The use of different beam profiles allows one to capture how variations in the intensity distribution influence the confinement experienced by the electron.

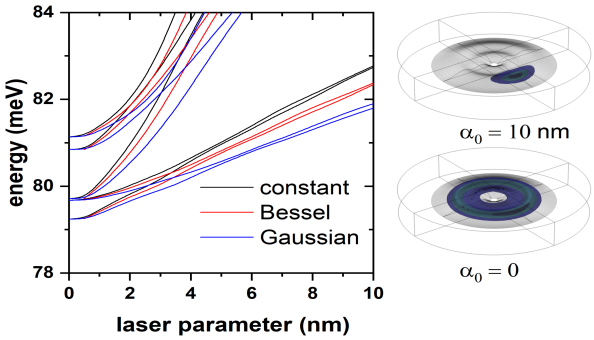

Fig. 4. Lowest electronic energy levels as a function of the laser parameter α0 for the Kuroda-type double-ring structure. The black curves correspond to a spatially uniform (constant) laser field, while the red and blue curves represent Bessel and Gaussian beams, respectively. The laser field is linearly polarized along the x direction.

Figure 4 shows the evolution of the lowest electronic energy levels as a function of the laser parameter α_0 for the Kuroda-type double-ring structure, together with the corresponding ground-state wavefunctions for $\alpha_0 = 0$ and $\alpha_0 = 10$ nm. As in Figure 3, all energy levels increase with α_0, indicating an overall strengthening of the confinement. However, in the double-ring system the behavior is more complex, as reflected in the different slopes and non-uniform separation between the energy branches. The wavefunction analysis provides additional insight into this behavior. In the absence of the laser field ($\alpha_0 = 0$), the ground-state wavefunction is distributed along the ring, preserving the circular symmetry of the system. When the laser field is applied ($\alpha_0 = 10$ nm), the electron remains confined within the same ring region, and no transfer to the inner ring is observed. Instead, the main effect of the laser is a redistribution of the probability density along the ring. The wavefunction becomes anisotropic, reflecting the linear polarization of the laser field along the x direction. This breaks the azimuthal symmetry and leads to a preferential localization of the electron along specific regions of the ring. This modification of the spatial distribution explains the changes observed in the energy spectrum. The variation in the slopes of the energy levels is associated with the adjustment of the electronic states to the anisotropic confinement induced by the laser field, rather than with a change in the radial localization of the electron. Compared to the single-ring case (Figure 3), the double-ring geometry enhances the sensitivity of the system to the spatial

© Ariston Publications 2026. All rights reserved.

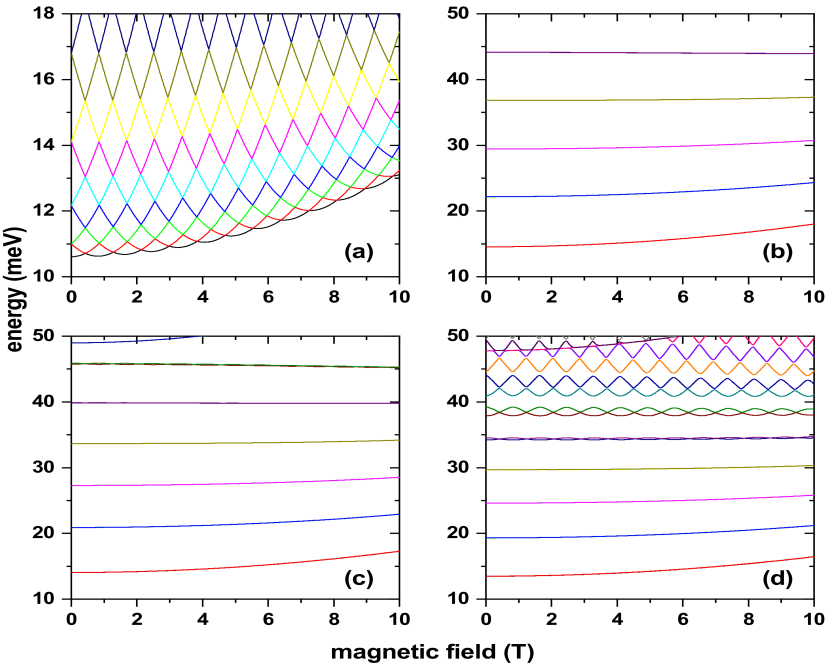

Fig. 5. Electronic energy levels as a function of the magnetic field for a quantum ring with inner radius 30 nm and outer radius 50 nm. (a) Without laser field, (b) constant laser field, (c) Bessel beam, and (d) Gaussian beam. The laser parameter is fixed at $\alpha_0 = 10$ nm.

structure of the laser field. However, the results show that, within the range of parameters considered, the laser primarily modifies the angular distribution of the wavefunction while preserving its radial confinement.

Figure 5 shows the evolution of the electronic energy levels as a function of the magnetic field for a quantum ring with inner radius 30 nm and outer radius 50 nm. Four cases are considered: (a) absence of laser field, (b) constant laser field, (c) Bessel beam, and (d) Gaussian beam, with a fixed laser parameter $\alpha_0 = 10$ nm. In the absence of the laser field (Figure 5 a), the energy levels exhibit a clear oscillatory behavior as a function of the magnetic field. The oscillatory behavior is characteristic of quantum ring systems and reflects the sensitivity of the energy levels to the magnetic flux threading the ring. When the laser field is introduced, the behavior changes significantly. For the constant laser field (Figure 5 b), the energy levels become almost linear with the magnetic field. This indicates a loss of the ring-like behavior, and the system effectively transitions toward a quantum dot--like regime. In this case, the electron no longer exhibits a well-defined ring-like character, and the system approaches a quantum dot--like behavior. A similar trend is observed for the Bessel beam (Figure 5 c), although small deviations from linearity remain. The structured spatial profile of the Bessel beam partially preserves some features of the ring geometry, but the overall behavior is still dominated by a stronger effective confinement. In contrast, for the Gaussian beam (Figure 5d), the behavior depends on the energy range. For lower energy states, the evolution is closer to linear, indicating a reduced influence of the ring geometry. However, for higher energy states, oscillatory features reappear. This suggests that these states remain sensitive to the ring geometry and retain a degree of ring-like character. The differences between these cases are directly related to the spatial distribution of the laser field. In general, the presence of the laser modifies the effective potential and reduces the contribution of azimuthal symmetry to the electronic states. Moreover, since the laser field is linearly polarized along the x-direction, the azimuthal symmetry of the system is broken. This symmetry breaking leads to anisotropic confinement, which further suppresses the characteristic ring behavior. In the present case, the laser field not only changes the confinement strength but also the nature of the electronic states, driving a transition from ring-like to dot-like behavior depending on the laser profile and the energy range.

Figure 6 shows the evolution of the electronic energy levels as a function of the magnetic field for the Kuroda-type double-ring structure. As in Figure 5, four cases are considered: (a) without laser field, (b) constant laser field, (c) Bessel beam, and (d) Gaussian beam, with a fixed laser parameter $\alpha_0 = 10$

 © Ariston Publications 2026. All rights reserved.

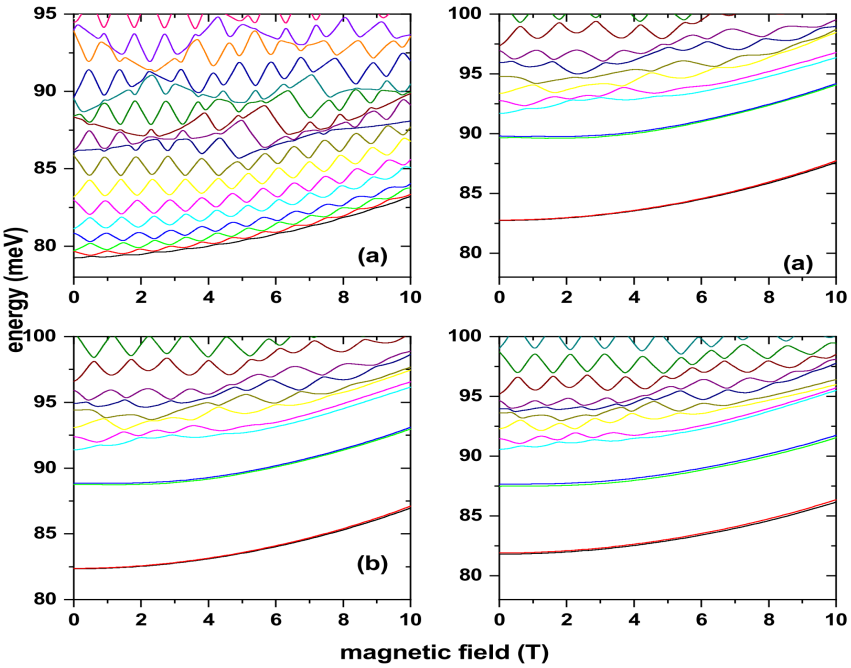

Fig. 6. Electronic energy levels as a function of the magnetic field for a Kuroda-type double quantum ring. (a) Without laser field, (b) constant laser field, (c) Bessel beam, and (d) Gaussian beam. The laser parameter is fixed at $\alpha_0 = 10$ nm.

nm. In the absence of the laser field (Figure 6 a), the energy levels exhibit clear oscillatory behavior, characteristic of ring-like systems. In this case, two distinct groups of oscillating branches can be identified. The lower-energy set is mainly associated with states localized in the outer ring, while a second group at higher energies can be attributed to states influenced by the inner ring. This reflects the presence of two confinement regions in the structure. When the laser field is introduced, the behavior becomes more complex. For the constant laser field (Figure 6 b), the lowest energy levels show a nearly linear dependence on the magnetic field, indicating a reduction of the ring-like character for states associated with the outer ring. However, a higher-energy group still exhibits oscillatory features, which can be linked to states influenced by the inner ring. A similar interpretation applies to the Bessel beam (Figure 6 c). Although the laser modifies the spectrum, oscillatory behavior is still clearly visible in a wide range of energies. The presence of distortions or irregularities in some branches can be associated with the contribution of the inner ring, which introduces additional structure in the spectrum. For the Gaussian beam (Figure 6 d), the spectrum shows a combination of smooth and oscillatory behavior. Lower energy levels tend to evolve more smoothly, while higher-energy states retain oscillations. As in the previous cases, the distorted or more structured branches are related to the influence of the inner ring, whose confinement leads to additional modulation of the energy levels.

Overall, two distinct regimes can be identified in the double-ring system. For the laser-dressed case ($\alpha_0 = 10$ nm), the confinement is strongly modified and the system tends to behave as a set of quantum dot--like states distributed along the outer ring. In this regime, the low-energy spectrum is mainly governed by the outer ring, which dominates the electronic localization. However, at higher energies, additional features appear that cannot be attributed solely to the outer ring. These features, including extra branches and distortions in the spectrum, indicate the contribution of the inner ring. As a result, the high-energy region reflects a combined effect of both confinement regions, where the outer ring provides the dominant contribution while the inner ring introduces additional structure in the spectrum.

4. CONCLUSION

In this work, we investigated the electronic properties of single and double quantum ring systems under the combined influence of magnetic and intense nonresonant laser fields. Special attention was given to the role of the laser spatial profile by considering constant, Gaussian, and Bessel distributions. For the ideal two-dimensional quantum ring, the magnetic

© Ariston Publications 2026. All rights reserved.

field produces the characteristic oscillatory behavior associated with ring-like confinement. However, when the laser intensity increases, the azimuthal symmetry is progressively broken due to the linear polarization along the x-direction. As a consequence, the electron localization changes along the ring and the energy spectrum evolves toward a quantum dot-like behavior with a nearly linear dependence on the magnetic field. This effect is observed for all laser profiles, although the confinement modification depends on the spatial distribution of the optical field. In the Kuroda-type double-ring structure, the electronic behavior becomes more complex due to the coexistence of inner and outer confinement regions. Under strong laser fields, the low-energy states are mainly governed by the external ring, while higher-energy states 7 exhibit additional spectral branches and distortions associated with the contribution of the inner ring. Therefore, the high-energy part of the spectrum reflects a combined effect of both confinement regions. The results also show that the laser field mainly modifies the angular distribution of the electronic states without producing a direct transfer of the electron between rings. Overall, the interplay between magnetic confinement, realistic ring geometries, and structured laser profiles provides an effective mechanism for controlling the electronic structure of semiconductor quantum ring systems.

DECLARATIONS

Acknowledgments

J.A. Vinasco acknowledges the support from the Universidad Nacional de Colombia, Sede Palmira, for the development of this research. J. Sierra-Ortega and G.E. Escorcia-Salas acknowledge the support from the Universidad del Magdalena.

Ethical Approval

We affirm that this manuscript is an original work, has not been previously published, and is not currently under consideration for publication in any other journal or conference proceedings. All authors have reviewed and approved the manuscript, and the order of authorship has been mutually agreed upon.

Funding

Funding not available

Availability of data and material

The datasets used and/or analyzed during the current study are available from the corresponding author on reasonable request.

Conflicts of Interest

The authors declare that they have no financial or personal interests that could have influenced the research and findings presented in this paper. The authors alone are responsible for the content and writing of this article.

Authors' contributions

Conceptualization, J.A.V., J.S.O., and G.E.E.S; **Methodology**, J.A.V., J.S.O., and G.E.E.S; **Software**, C.F.V., F.G.A., J.A.V., J.S.O., and G.E.E.S; **Validation**, J.A.V., J.S.O., and G.E.E.S; **Formal analysis**, C.F.V., J.A.V., J.S.O., and G.E.E.S; **Investigation**, C.F.V., F.G.A., J.A.V., J.S.O., and G.E.E.S; **Data curation**, C.F.V., F.G.A., J.A.V., J.S.O., and G.E.E.S; **Writing—original draft preparation**, C.F.V., F.G.A., J.A.V., J.S.O., and G.E.E.S; **Writing—review and editing**, C.F.V., F.G.A., J.A.V., J.S.O., and G.E.E.S; **Supervision**, J.A.V., J.S.O., and G.E.E.S; **Project administration**, J.A.V., J.S.O., and G.E.E.S. All authors have read and agreed to the published version of the manuscript.

REFERENCES

[1] Jayan, J. S. and Raman, A. and Kumar, S. S. and Saigayathri, M. and Parameswaranpillai, J. and Punetha, V. D. and Saritha, A., **2026**. Recent breakthroughs in quantum dot photocatalysis: a critical appraisal. *Fuel*, 425, p.139432. https://doi.org/10.1016/j.fuel.2026.139432.

[2] Dolatyari, M. and Rostami, A. and Yadav, A., **2026**. Doped semiconductor quantum dots: From controlled synthesis and optical engineering to bioimaging and theranostic applications. *Materials Today Chemistry*, 54, p.103653. https://doi.org/10.1016/j.mtchem.2026.103653.

[3] Wang, B. and Yang, Q. and Mu, B., **2026**. A multifunctional coating based on carbon quantum dots. *Materials Science and Engineering B*, 330, p.119491. https://doi.org/10.1016/j.mseb.2026.119491.

[4] Ouaridhine, A. and Aissat, A. and Wadi, M. and Benamar, M. A. and Dupont,

 © Ariston Publications 2026. All rights reserved.

S., **2026**. Modeling and simulation of the InGaAs/Si quantum dot structure for solar cells applications. *Journal of the Indian Chemical Society*, 103, p.102657. https://doi.org/10.1016/j.jics.2026.102657.

[5] Aharonov, Y. and Bohm, D., **1959**. Significance of electromagnetic potentials in the quantum theory. *Physical Review*, 115(3), p.485-491. https://doi.org/10.1103/PhysRev.115.485.

[6] Ali, A. A. and Shaer, A. and Elsaid, M., **2022**. Simultaneous effects of Rashba, magnetic field and impurity on the magnetization and magnetic susceptibility of a GaAs-semiconductor quantum ring. *Journal of Magnetism and Magnetic Materials*, 556, p.169435. https://doi.org/10.1016/j.jmmm.2022.169435.

[7] Mehramiz, A. and Pasandideh, K. and Alijabbari, M., **2024**. The electronic properties of a single electron in the GaAs/Ga1−xAlxAs oblate spheroidal quantum dot under the finite confinement potential. *Physics Letters A*, 528, p.130035. https://doi.org/10.1016/j.physleta.2024.130035.

[8] Balakirev, S. V. and Solodovnik, N. E. and Kirichenko, D. V. and Dukhan, D. D. and Shandyba, N. A. and Eremenko, M. M. and Solodovnik, M. S., **2026**. Epitaxial realization of triple InAs/GaAs quantum dots in a triangular arrangement. *Materials Science in Semiconductor Processing*, 211, p.110747. https://doi.org/10.1016/j.mssp.2026.110747.

[9] Castrillón, J. D. and Gómez-Ramírez, D. A. J. and Rivera, I. E. and Suaza, Y. A. and Marín, J. H. and Fulla, M. R., **2020**. Artificial Hydrogen molecule in vertically stacked Ga1−xAlxAs nanoscale rings: Structural and external probes effects on their quantum levels. *Physica E*, 117, p.113765. https://doi.org/10.1016/j.physe.2019.113765.

[10] Ospina, D. A. and Duque, D. and Mora-Ramos, M. E. and Vinasco, J. A. and Radu, A. and Restrepo, R. L. and Morales, A. L. and Sierra-Ortega, J. and Escorcia-Salas, G. E. and Giraldo, M. A. and Montoya-Sanchez, J. and Duque, C. A., **2024**. Hopf-link GaAs-AlGaAs quantum ring under geometric and external field settings. *Physica E*, 163, p.116032. https://doi.org/10.1016/j.physe.2024.116032.

[11] Hahn, R. V. H. and Montoya-Sánchez, J. and Vinasco, J. A. and Mora-Ramos, M. E. and Duque, C. A., **2025**. Structural modifications in GaAs/AlGaAs tetrapod nanocrystals under applied pressure and temperature: Electron-impurity properties. *Physics Letters A*, 558, p.130897. https://doi.org/10.1016/j.physleta.2025.130897.

[12] Hoa, L. T. and Hieu, N. N. and Bich, T. N. and Hoa, V. T. and Phuc, H. V., **2026**. Excited-state optical absorption in modified Kratzer–ring-shaped quantum dots. *Physica B*, 730, p.418495. https://doi.org/10.1016/j.physb.2026.418495.

[13] Arraoui, R. and Jaouane, M. and El-Hamouchi, J. and Fakkahi, A. and Mazouz, A. and Ed-Dahmouny, A. and Sali, A., **2026**. Tuning second and third harmonic generation in GaAs/AlxGa1−xAs four quantum dot nanostructures. *Materials Research Bulletin*, 202, p.114165. https://doi.org/10.1016/j.materresbull.2026.114165.

[14] Holskyi, V. B. and Leshko, R. Ya. and Karpiy, V. R. and Holskyi, K. V., **2026**. Electronic states in a linear quantum molecule of four spherical quantum dots. *Physica B*, 731, p.418480. https://doi.org/10.1016/j.physb.2026.418480.

[15] Bejan, D. and Stan, C., **2024**. Controlling the interband transitions in a triple quantum ring: Effects of intense laser and electric fields. *Journal of Physics and Chemistry of Solids*, 188, p.111887. https://doi.org/10.1016/j.jpcs.2024.111887.

[16] Ed-Dahmouny, A. and Zeiri, N. and Jahromi, H. D. and Baser, P. and Jaouane, M. and Sali, A. and Duque, C. A. and Wong, B. M., **2026**. Machine learning for predicting temperature-driven nonlinear optical rectification in tetrapod core/shell quantum dots. *Materials Today Communications*, 52, p.115169. https://doi.org/10.1016/j.mtcomm.2026.115169.

[17] A, F. K. and Ravindran, S. and Park, K. and Alameh, K. and Bengi, A. and V, H. A. and Lee, Y. T., **2020**. Advanced realization and characterization of directed optical logic gates using electroabsorptive quantum-well-based micro ring resonator. *Optik*, 221, p.164426. https://doi.org/10.1016/j.ijleo.2020.164426.

© Ariston Publications 2026. All rights reserved.

[18] Hadi, M. E. and Hbibi, M. and Chouef, S. and Boussetta, R. and Moussaouy, A. E. and Mommadi, O. and Duque, C. A., **2026**. Study of the electronic properties of quantum rings under the influence of the electric field in the presence of two off-center impurities. *Scientific African*, 31, p.e03155. https://doi.org/10.1016/j.sciaf.2025.e03155.

[19] Hasanirokh, K. and Al, E. B. and Tuzemen, A. T. and Sayrac, M. and Sayrac, H. and Ungan, F., **2025**. Investigation of nonlinear optical properties in GaAs/GaAlAs quantum well with modified Lennard-Jones potential: Role of static electromagnetic fields, intense laser radiation and structure parameters. *Photonics and Nanostructures*, 65, p.101403. https://doi.org/10.1016/j.photonics.2025.101403.

[20] Sedehi, H. R. R. and Bazrafshan, A. and Khordad, R., **2022**. Thermal properties of quantum rings in monolayer and bilayer graphene. *Solid State Communications*, 353, p.114853. https://doi.org/10.1016/j.ssc.2022.114853.

[21] Henneberger, W. C., **1968**. Perturbation method for atoms in intense light beams. *Physical Review Letters*, 21(12), p.838-841. https://doi.org/10.1103/PhysRevLett.21.838.

[22] Al-Naghmaish, A. and Dakhlaoui, H. and Ghrib, T. and Wong, B. M., **2022**. Effects of magnetic, electric, and intense laser fields on the optical properties of AlGaAs/GaAs quantum wells for terahertz photodetectors. *Physica B*, 635, p.413838. https://doi.org/10.1016/j.physb.2022.413838.

[23] Suaza, Y. A. and Fulla, M. R. and Pérez-Taborda, J. A. and Avila, A. and Lafaurie-Ponce, L. G. and Marín, J. H., **2022**. Intense laser field effect on the D+2 molecular complex strongly confined in a semiconductor quantum ring: Electronic and optical properties. *Optics and Laser Technology*, 152, p.108134. https://doi.org/10.1016/j.optlastec.2022.108134.

[24] Gavalajyan, S. P. and Mantashyan, P. A. and Kazaryan, E. M. and Danielyan, G. and Vinnichenko, M. Y. and Zeiri, N. and Duque, C. A. and Hayrapetyan, D. B. and Sargsian, T. A., **2026**. Bessel-beam-assisted persistent current in toroidal semiconductor quantum dots. *Materials Today Communications*, 51, p.114781. https://doi.org/10.1016/j.mtcomm.2026.114781.

[25] García, J. M. and Medeiros-Ribeiro, G. and Schmidt, K. and Ngo, T. and Feng, J. L. and Lorke, A. and Kotthaus, J. and Petroff, P. M., **1997**. Intermixing and shape changes during the formation of InAs self-assembled quantum dots. *Applied Physics Letters*, 71(14), p.2014-2016. https://doi.org/10.1063/1.119772.

[26] Kuroda, T. and Mano, T. and Ochiai, T. and Sanguinetti, S. and Sakoda, K. and Kido, G. and Koguchi, N., **2005**. Optical transitions in quantum ring complexes. *Physical Review B*, 72(20), p.205301. https://doi.org/10.1103/PhysRevB.72.205301.

 © Ariston Publications 2026. All rights reserved.